

Fast Dynamics of a Hydrogen-Bonding Glass Forming Liquid: Chemical Exchange-Induced Spectral Diffusion in 2D IR Spectroscopy

David J. Hoffman, Sebastian M. Fica-Contreras, and Michael D. Fayer*

Department of Chemistry
Stanford University, Stanford, CA 94305
*Phone: 650 723-4446; Email: fayer@stanford.edu

Supplemental Material

S1. Jump Exchange Kinetic Model

S2. Determining the Line Shape Parameters

S3. Calculating the XISD Line Shapes

S4. Implementing the Homogeneous “Wobbling” Model

S5. Implementing Heterogeneous Orientational Relaxation/Chemical Exchange

S6. Fit Method Details

S7. Additional Notes on Temperature Dependent Parameters

S8. Plots of Homogeneous and Heterogeneous Model Fits at All Temperatures

S1. Jump Exchange Kinetic Model

The theory of jump chemical exchange in 2D IR spectroscopy was developed in detail by Ji and Gaffney,¹ but the relevant results are presented and extended here. For our proposed two-state system (the H-bonding (HB) and non-bonding (NB) species) the populations obey the following analytic equations:

$$\begin{pmatrix} N_{HB}(t) \\ N_{HB}^*(t) \\ N_{NB}^*(t) \\ N_{NB}(t) \end{pmatrix}_{XXXX} = \frac{1}{3} \begin{pmatrix} e^{-A \cdot t} + \frac{4}{5} e^{-B \cdot t} \\ e^{-A \cdot t} - \frac{2}{5} e^{-B \cdot t} \end{pmatrix} \begin{pmatrix} N_{HB}(0) \\ N_{HB}^*(0) \\ N_{NB}^*(0) \\ N_{NB}(0) \end{pmatrix} \quad (S1)$$

$$\begin{pmatrix} N_{HB}(t) \\ N_{HB}^*(t) \\ N_{NB}^*(t) \\ N_{NB}(t) \end{pmatrix}_{YYYY} = \frac{1}{3} \begin{pmatrix} e^{-A \cdot t} + \frac{4}{5} e^{-B \cdot t} \\ e^{-A \cdot t} - \frac{2}{5} e^{-B \cdot t} \end{pmatrix} \begin{pmatrix} N_{HB}(0) \\ N_{HB}^*(0) \\ N_{NB}^*(0) \\ N_{NB}(0) \end{pmatrix}$$

Where

$$\mathbf{A} = \begin{pmatrix} k_{HB} + k_{HB-NB} & & & \\ & k_{HB} + k_{HB-NB} & -k_{NB-HB} & -k_{NB-HB} \\ -k_{HB-NB} & -k_{HB-NB} & k_{NB} + k_{NB-HB} & \\ & & & k_{NB} + k_{NB-HB} \end{pmatrix}$$

$$\mathbf{B} = \begin{pmatrix} k_{HB} + k_{HB-NB} + 6D_{HB} & & & \\ & k_{HB} + k_{HB-NB} + 6D_{HB} & -\langle P_2(\cos \Theta) \rangle k_{NB-HB} & -\langle P_2(\cos \Theta) \rangle k_{NB-HB} \\ -\langle P_2(\cos \Theta) \rangle k_{HB-NB} & -\langle P_2(\cos \Theta) \rangle k_{HB-NB} & k_{NB} + k_{NB-HB} + 6D_{NB} & \\ & & & k_{NB} + k_{NB-HB} + 6D_{NB} \end{pmatrix} \quad (\text{S2})$$

Here, N_{HB} and N_{NB} are the time-dependent populations of the H-bonding and non-bonding populations respectively, \mathbf{A} is the isotropic exchange matrix and \mathbf{B} is the anisotropic exchange matrix. The contributions of these matrices can be isolated with simple manipulations of Eq. S1, with:

$$\begin{aligned}
\mathbf{N}_{Iso} &= \mathbf{N}_{XXXX} + 2\mathbf{N}_{XXYY} = e^{-\mathbf{A} \cdot t} \\
\mathbf{N}_{Aniso} &= \mathbf{N}_{XXXX} - \mathbf{N}_{XXYY} = \frac{2}{15} e^{-\mathbf{B} \cdot t}
\end{aligned} \quad (\text{S3})$$

This is equivalent to obtaining the experimental isotropic ($\langle XXXX \rangle + 2\langle XXYY \rangle$) and anisotropic ($\langle XXXX \rangle - \langle XXYY \rangle$) 2D spectra through linear combinations of the parallel and perpendicular 2D spectra.

Both N_{HB} and N_{NB} are further subdivided into populations that have undergone exchange (denoted with a * superscript) and have not undergone exchange (no superscript). This subdivision is a straightforward modification of the kinetic equations as previously described by Ji and Gaffney, who were interested in the amplitudes of the 2D bands but not their shapes. The subdivision is critically important for describing the overall line shape, as we need to be able to rigorously distinguish between the non-exchanged populations which have non-zero FFCFs and populations after exchange, for which the FFCF is zero. There is otherwise no chemical or spectroscopic difference between the N and N^* populations. From this definition, we can also see that both the HB and NB initial subensembles, $N^* = 0$ at $t = 0$.

\mathbf{A} is made up of k_{HB} and k_{NB} , which are the population relaxation rates (vibrational lifetimes) for the two species, and k_{HB-NB} and k_{NB-HB} which are the rates of chemical exchange

between the two species. 2D IR is a non-perturbative measurement, meaning that the experiment probes the equilibrium fluctuations between populations also at equilibrium. This introduces the additional constraint of

$$(N_{HB} + N_{HB}^*)k_{HB-NB} = (N_{NB} + N_{NB}^*)k_{NB-HB} . \quad (\text{S4})$$

The \mathbf{B} matrix additionally has D_{HB} and D_{NB} , which are the orientational diffusion constants for the two species (multiplied by 6 as the experiments measure the C_2 correlation time), and Θ , which is the aforementioned “jump” angle associated with the exchange. When $\Theta = 0$, the equations simplify to the chemical exchange equations described in Kwak *et al.*²

To determine the overall intensities of the diagonal and cross peaks, it is necessary to also introduce the relative transition dipoles, μ_{HB} and μ_{NB} , of the two species. Further, by replacing the population vector in Eq. S1 with a density matrix, it is possible to track the initial and final state of populations with respect to time. Thus replacing Eq. S1 with expressions of the form

$$\mathbf{N}(t) = \frac{1}{3} \begin{pmatrix} |\mu_{HB}|^2 & & & \\ & |\mu_{HB}|^2 & & \\ & & |\mu_{NB}|^2 & \\ & & & |\mu_{NB}|^2 \end{pmatrix} (e^{-\mathbf{A}t} + ae^{-\mathbf{B}t}) , \quad (\text{S5})$$

$$\times \begin{pmatrix} |\mu_{HB}|^2 & & & \\ & |\mu_{HB}|^2 & & \\ & & |\mu_{NB}|^2 & \\ & & & |\mu_{NB}|^2 \end{pmatrix} \begin{pmatrix} N_{HB}(0) & & & \\ & 0 & & \\ & & 0 & \\ & & & N_{NB}(0) \end{pmatrix}$$

where $a = 4/5$ for an $\langle \text{XXXX} \rangle$ pulse sequence and $-2/5$ for an $\langle \text{XXYY} \rangle$ pulse sequence, as in Eq. S1. From here it is possible to read off the relative intensities of the different peaks from the time dependent density matrix. For instance, all populations that begin the waiting period H-bonded will be in column 1, with those that do not exchange by time t in row 1 (diagonal peak), those that exchanged once (or an odd number of times) in row 3 (exchange peak), and those that have exchanged an even number of times in row 2 (decorrelated diagonal peak).

S2. Determining the Line Shape Parameters

While the kinetic model tells us the relative intensity of the peaks, it is necessary to compute the overall line shape to model the observables. The 2D line shapes are calculated numerically using the response functions reported in Kwak *et al.*² Examples of calculated component line shapes are given in Fig. 6. The desired total line shape of a specific peak is a particular linear combination of these six component peaks. One contribution to the diagonal peaks is from the subensembles of molecules that have not undergone chemical exchange. These subensembles exhibit normal spectral diffusion. However, subensembles that have undergone an even number of exchanges will give a completely decorrelated contribution to the diagonal peaks. Subensembles that have undergone an odd-numbered of exchanges form the off-diagonal peaks, which will have a decorrelated 2D line shape.² These overlapping exchange peaks have polarization dependent intensities, which will distort the total line shape differently in the two different polarizations and effect the CLS observable accordingly. After determining the impact of the exchange peaks on the CLS measurements, the remaining structural spectral diffusion in the diagonal peaks can also be calculated.

A proper description of the peaks requires good information on the center frequencies, inhomogeneous widths, and homogeneous widths of the two populations. From the two component fit to the vibrational lifetime and the two-peak fit of the linear FT-IR spectra, it is possible to get reasonable values for the center frequencies and total widths of the two component peaks from the Gaussian fits to the spectrum. The anharmonic shift (energy difference between 0 to 1 and 1 to 2 transitions) can also be directly calculated by the difference in frequency between the relevant minimum and maximum in the isotropic pump-probe decomposition (Fig. 2). These results are summarized in Table 1.

The overall dephasing time, T_2 (homogeneous dephasing), can be extracted directly from the vibrational echo at short times by measuring the decay time of the time domain interferogram's envelope.³ As the broad, H-bonded peak is the dominant part of the two-component fits (see Fig. 2), and the observed T_2 is much shorter than seen in non-H-bonding glass formers at analogous temperatures, it is assumed that the observed T_2 is mostly due to the H-bonding peak (as reported in Table 3). The dephasing time of the non-H-bonding peak was chosen to be identical to that of PhSeCN in other non-H-bonding glass formers at the same rescaled temperature relative to their respective T_g 's (values in Table 4).^{3,4} This rescaling was found to be valid for non-hydrogen bonding glass formers BZP and OTP. With the dephasing

time (homogeneous width) determined, it is then straightforward to predict the size of the inhomogeneous component that gives the correct total linewidth for each subpopulation by using an analytic approximation to a Voigt line shape.

The remaining time-independent terms that are needed to describe the total line shape are the relative equilibrium population sizes and relative transition dipoles. The intensity of the linear FT-IR spectrum depends linearly on population and on the transition dipole squared, while the intensity of the third-order pump probe (or 2D IR) signal is also linear in the population but depends on the transition dipole to the fourth power.⁵ By simultaneously fitting the linear spectrum and an early time pump-probe spectrum (before chemical exchange takes place), it is possible to determine both the relative populations and transition dipoles as reported in Table 1. It was found that modest adjustments to the relative dipole ratios did not substantially change the overall fit results.

S3. Calculating the XISD Line Shapes

At this point, the time dependent terms, the rates and jump angle in the kinetic model as well as the frequency amplitudes and time constants in the FFCF of the HB and NB populations, need to be determined. As is clearly seen from the experimental data, these parameters will generally be highly temperature dependent. While there is a large parameter space, as there are potentially two vibrational lifetimes, two orientational diffusion constants, an exchange rate and jump angle, and (by assumption from previous experiments) two components with two time constants in the FFCF, the problem is constrained by having four time dependent data sets to fit: the $\langle XXXX \rangle$ and $\langle XXYY \rangle$ CLS from the 2D IR datasets and the corresponding isotropic and anisotropic pump-probe signals.

The 2D IR data is simulated by first solving Eq. S5 for a given T_w and polarization to determine the relative amplitudes of the diagonal and cross peaks. The non-exchange contributions to the diagonal peaks are also calculated from the values of their FFCFs for the given T_w . As it is very computationally expensive to calculate an entire dataset's worth of 2D line shapes (frequently over 50 T_w 's were used), a large set of 2D line shapes was pre-calculated for a wide range of potential FFCF's from fully correlated to fully decorrelated. For a given trial FFCF, the program would then find the closest match for the value of the FFCF at that T_w and make the relevant linear combinations with the other peaks, per Eq. S5. This method reduced the

computation time for a trial set of parameters from several minutes to under a second. The T_w and polarization dependent CLS can then be calculated in the same manner as used for an experimental 2D spectrum. When properly implemented, this technique is capable of reproducing the experimental line shapes very well (Fig. 7).

The pump-probe data is then calculated by numerically integrating along the ω_1 axis of the 2D spectra (per the projection-slice theorem⁵), and the isotropic and anisotropic components are determined by Eq. 1. By calculating the pump-probe decays in this manner, the frequency dependence (or lack thereof) can also be examined to extract the kinetics of the subcomponents.

S4. Implementing the Homogeneous “Wobbling” Model

In terms of the wobbling-in-a-cone model,^{6, 7} the orientational relaxation is given by

$$C_2(t) = T^2 \left(S^2 + (1 - S^2) \exp(-t / \tau_{wob}) \right) \exp(-t / \tau_D) = C_2^{wob}(t) \exp(-t / \tau_D), \quad (S6)$$

where $\tau_D = 1/6D_{or}$, for orientational diffusion constant D_{or} , and T and S are order parameters of the form

$$Q = \frac{1}{2} \cos \theta_0 (1 + \cos \theta_0), \quad (S7)$$

with a cone half-angle of θ_0 .

Wobbling-in-a-cone is introduced into the kinetic equations by making the orientational diffusion rates (D_{HB} and D_{NB}) time dependent, in the same manner as Ji and Gaffney.¹ Eq. S6 is cast in the form of a diffusion equation with a new, time-dependent rate $D_{eff}(t)$:

$$\begin{aligned} \frac{d}{dt} C_2(t) &= -6D_{eff}(t)C_2(t) \\ 6D_{eff}(t) &= 6D_{or} - \frac{d}{dt} \ln [C_2^{wob}(t)] \approx 6D_{or} - \ln [C_2^{wob}(t)] / t \end{aligned}, \quad (S8)$$

where the latter approximation holds as long as $\tau_{wob} \ll \tau_D$. The approximation for D_{eff} is then directly substituted into the anisotropic \mathbf{B} matrix for D_{or} (specifically D_{HB} and D_{NB}). While this makes the \mathbf{B} matrix time-dependent, the approximation eliminates the need for numerical integration of the rate equations.

The lack of a frequency dependence for the anisotropy also implies that the wobbling behavior would have to be the same for both H-bonded and non-bonded probes. We can use this

observation to further constrain the influx of new parameters, as T^2 , S^2 , and τ_{wob} will have to be approximately identical in both species.

We can now use nonlinear fitting methods to calculate the best fit parameters for a given temperature. As was discussed in the main text, we will first use a data set at moderate supercooling that shows large differences between the $\langle \text{XXXX} \rangle$ and $\langle \text{XXYY} \rangle$ CLS curves to obtain the magnitudes of the parameters. In addition to the results reported in the main text (orientational diffusion arises virtually entirely from chemical exchange, and the systematic lack of agreement at intermediate times), a few other additional features were found. First, the population decay times ($1/k_{HB}$ and $1/k_{NB}$) match very closely to those was measured with the two-component fit of the population decay, giving 225 and 480 ps respectively. These terms were used for all of the remaining fits. As the population sizes are similar (Table 1), the impact of differing exchange rates are relatively minimal on the observed population decays, explaining why the population decays are generally temperature independent. In addition, the orientational relaxation measured by the pump-probe anisotropy is modeled well (Fig. 8B, blue curve).

S5. Implementing Heterogeneous Orientational Relaxation/Chemical Exchange

For the first model (top of Fig. 9), in which there is no interconversion between domains with fast and slow dynamics on the timescale of the 2D IR experiment, the modification is straightforward. The population is split as

$$\mathbf{N}_{\text{tot}}(t) = (1-f)\mathbf{N}_{\text{fast}}(t) + f\mathbf{N}_{\text{slow}}(t) \quad (\text{S9})$$

where both N_{fast} and N_{slow} are described by Eq. S5, with the only difference being in the values of exchange rates $1/k_{NB-HB}$ and $1/k_{HB-NB}$ in the \mathbf{A} and \mathbf{B} matrices. The number of free parameters in the model is the same as in the “wobbling-in-a-cone” model, with the “fast” exchange rate serving the role of τ_{wob} and f serving the role of S^2 . It is necessary to keep the subpicosecond inertial term, T^2 , as it was introduced in Eq. S6, to describe the deviation from perfect correlation at zero waiting time. This is done by using the modification in Eq. S8 but setting S^2 (which appears in C_2^{wob} via Eq. S6) equal to 1.

The second model (bottom of Fig. 9) requires substantial modifications. To maintain the same number of parameters as the previous models, it is assumed that there is no chemical exchange between members of the slow population, essentially making them immobile until they

are moved into the fast population. All chemical exchange and reorientation occurs in the subensemble of “fast” liquid domains (fast dynamics in Fig. 9 bottom). The kinetic equations are then

$$\mathbf{N}(t) = \frac{1}{3} \begin{pmatrix} |\mu_{HB}|^2 & & & \\ & |\mu_{HB}|^2 & & \\ & & |\mu_{NB}|^2 & \\ & & & |\mu_{NB}|^2 \end{pmatrix} \left(e^{-\mathbf{A}t} + a e^{-\mathbf{B}t} \right) \begin{pmatrix} N_{HB,slow}(0) \\ N_{HB,fast}(0) \\ N_{NB,fast}(0) \\ N_{NB,slow}(0) \end{pmatrix} \quad (\text{S10})$$

Where the **A** and **B** matrices are now:

$$\mathbf{A} = \begin{pmatrix} k_{HB} + k_{act,HB} & -k_{deact,HB} & & \\ -k_{act,HB} & k_{HB} + k_{HB-NB} + k_{deact,HB} & -k_{NB-HB} & \\ & -k_{HB-NB} & k_{NB} + k_{NB-HB} + k_{deact,NB} & -k_{act,NB} \\ & & -k_{deact,NB} & k_{NB} + k_{act,NB} \end{pmatrix} \quad (\text{S11})$$

$$\mathbf{B} = \begin{pmatrix} k_{HB} + k_{act,HB} + 6D_{HB} & -k_{deact,HB} & & \\ -k_{act,HB} & k_{HB} + k_{HB-NB} + k_{deact,HB} + 6D_{HB} & -\langle P_2(\cos \Theta) \rangle k_{NB-HB} & \\ & -\langle P_2(\cos \Theta) \rangle k_{HB-NB} & k_{NB} + k_{NB-HB} + k_{deact,NB} + 6D_{NB} & -k_{act,NB} \\ & & -k_{deact,NB} & k_{NB} + k_{act,NB} + 6D_{NB} \end{pmatrix}$$

k_{act} corresponds to the rate of “slow” particles becoming “fast,” and k_{deact} corresponds to the rate of “fast” particles becoming “slow.” The N^* population distinctions (corresponding to the probe molecules that have undergone chemical exchange during the experiment) are neglected here for space but can be added in the same straightforward manner as before to yield 8x8 density matrices. We will hold the ratios, $N_{slow}/N_{tot} = f$, to be the same for both the HB and NB species, as was done in the first heterogeneous model. The exchange rate between the fast and slow dynamical populations was also assumed to be the same for the HB and NB chemical species,

again justified by the frequency independence of the pump-probe anisotropy. The fast and slow populations are taken to be in equilibrium. This latter fact gives

$$\begin{aligned} (N_{slow} + N_{slow}^*)k_{act} &= (N_{fast} + N_{fast}^*)k_{deact}; \\ k_{deact} &= \frac{f}{1-f}k_{act} \end{aligned} \quad (S12)$$

Making these assumptions again reduces the number of adjustable parameters to be identical to the homogeneous wobbling-in-a-cone model, as the heterogeneity is described completely by fraction f and the activation rate k_{act} . In comparisons to the first heterogeneous model, k_{act} corresponds to the slow exchange rate k_{NB-HB} . The other terms are directly analogous.

It is also assumed that the fast and slow populations have the same spectral diffusion dynamics; the spectral diffusion dynamics only depend on whether the species is HB or NB. In other words, being dynamically “fast” or “slow” refers only to whether the orientational relaxation and jump exchange is fast or slow. Orientational relaxation is determined by very local interactions of the probe molecule with its immediate environment. In contrast, spectral diffusion is caused by structural fluctuations on mesoscopic distance scales. For example, structural fluctuations occurring over a wide range of distances from the probe give rise to fluctuating electric fields, which can cause spectral diffusion through the vibrational Stark effect.⁸⁻¹⁰ The mesoscopic scale of spectral diffusion guarantees that the dynamically “fast” probes will exhibit some slow spectral diffusion, and vice versa.

S6. Fit Method Details

The homogeneous and the two heterogeneous kinetic models were employed to describe the pump-probe anisotropy and polarization-dependent CLS decays at a series of temperatures, 355 K to 270 K, from well above the melting temperature T_m through deep supercooling. As the isotropic pump-probe decay was found to be essentially temperature independent, the vibrational lifetimes of the two populations were held constant at the 225 and 480 ps values for the HB and NB species, respectively. The non-exchanging FFCFs were described as a biexponential for each species. These six FFCF parameters (1 amplitude and 2 time constants for each species’ FFCF) and the other five kinetic model parameters (exchange rate, jump angle, inertial cone, wobbling/fast time, wobbling cone/fast population) were allowed to vary. As having non-zero regular orientational diffusion rates (D_{HB} or D_{NB}) for either species did not improve the fits, the

two orientational diffusion parameters were held at zero for all temperatures. The insensitivity to D_{HB} or D_{NB} indicates that the dominant contribution to the pump-probe anisotropy decay is caused by the large-angle exchanges between the HB and NB species, i.e., reorientation of the PhSeCN probe is a result of the probe moving to a different chemical environment with a large angular jump.

As the pump-probe anisotropy only depends on the kinetic model, most of the parameters from the kinetic model can be obtained accurately. The inertial cone is set solely by the pump-probe anisotropy at $t = 0$, and the other terms, excluding the jump angle, can be obtained from a biexponential fit to the anisotropy. The jump angle Θ plays off against the exchange rate: a larger jump angle results in a slower exchange rate for the same anisotropy per Eq. 4.

As opposed to the kinetic model parameters, which can be accurately set through the anisotropy measurements, the parameters that define the SSD are more difficult to extract. The two bands are fully overlapped in both the $\langle XXXX \rangle$ and $\langle XXYY \rangle$ measurements, so the best fit parameters for the SSD of the HB and NB populations can compensate for each other to a degree. The more prominent HB contribution (see Fig. 2) is better defined than the relatively smaller NB contribution. Furthermore, as exchange occurs the relative amplitude of the non-exchanged SSD contribution to the diagonal bands decreases compared to those of the cross peaks and exchange contribution to the diagonal peaks. An example of the relative prominence of the peaks for the heterogeneous fit to the data at both polarizations at 290 K is illustrated in Fig. S1.

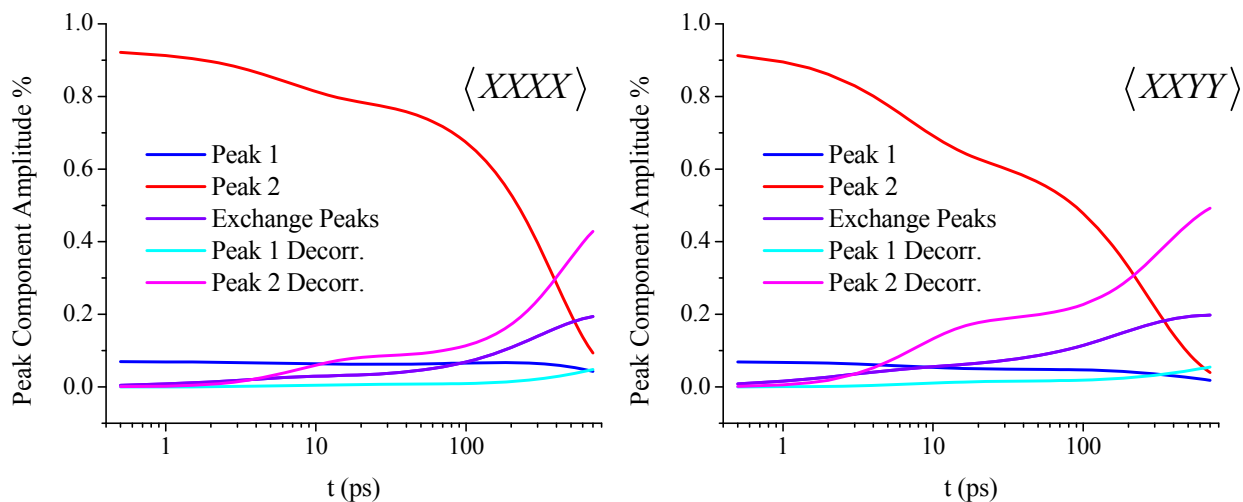


Fig. S1: Relative intensities of different peaks in the parallel and perpendicular pulse sequences for PhSeCN in 2BPM at 290 K fit with Heterogeneous Model 1.

Because of these amplitude effects, a range of SSD parameters will yield fits to the experimental data of similar quality. To attempt to quantify this uncertainty, the SSD fit parameters were initialized at a large number of values and allowed to converge to their local minima. The reported errors in Tables 2 through 5 are then the standard deviations of these collections of parameters from between 10 and 30 trials. Significantly increasing the number of trials was found to not dramatically change or lower the distribution of parameters.

S7. Additional Notes on Temperature Dependent Parameters

A. Vibrational Dephasing Times

As was discussed in Section S2, the dephasing time (T_2 in Eq. 2; see Table 3) of the HB species dramatically increases as the temperature is lowered. It follows the approximately T^2 power law temperature dependence that is characteristic of these liquids, which has previously been associated with Raman-like two-phonon scattering events.^{3, 11, 12} The dephasing time is faster (i.e., the homogeneous line is wider) than has been seen in non-H-bonding glass formers when temperature is rescaled relative to T_g , although it makes up an overall smaller fraction of the linewidth due to the much broader spectrum of the HB species. This results in the CLS starting closer to 1 at $T_w = 0$ at a given temperature.

As was discussed in Section S2, the dephasing time of the NB species (see Table 4) was assumed to have approximately the same behavior, following earlier results on non-hydrogen bonding supercooled liquids. The values that were employed are the dephasing times of PhSeCN in BZP when rescaled to the respective glass transition temperatures of 2BPM and BZP.

B. Inertial Cones

Sub-picosecond inertial motions appear in the pump-probe anisotropy as deviations from perfect correlation at zero waiting time, and is somewhat analogous to the effect of the dephasing time on the FFCF. As was mentioned in the main text and in Section S4, the frequency independence of the anisotropy says that the inertial wobbling must be essentially identical for the HB and NB species. It was found that the order parameter associated with this inertial motion, T^2 (not to be confused with the dephasing time T_2), increases monotonically with decreasing temperature, corresponding to greater confinement of the probe molecule on the shortest timescales. From Eq. S7, these order parameters corresponds to cone half-angles of 21° at the highest temperatures to 11° at the lowest temperatures.

C. Chemical Exchange Jump Angle

A potentially important consequence of a near-magic angle jump rate as was observed in the model fits is that it will suppress the appearance of cross peaks in the 2D anisotropic spectra. The suppressed cross peaks result in a spectra that primarily includes the non-exchanging populations. In principle, this could permit a more accurate determination of the SSD of these species, although it is similarly difficult to obtain high quality 2D anisotropic spectra for accurate line shape determination, especially at long T_w 's where it would be most valuable. Further, fits to the simulated and experimental 2D anisotropies did yield good matches for the heterogeneous models (Fig. 8C) without further parameter adjustments.

D. Comparison to the Parameters from the Homogeneous “Wobbling” Model

While the heterogeneous models were found to be either equivalent or superior at all temperatures, it is worth comparing to the analogous homogeneous model to test the robustness of the overall temperature dependence of the model. The kinetic model parameters for the homogeneous model are listed in Table S1. All of the timescales involved, in both the kinetic model and in the SSDs, were found to be essentially conserved between the two parameters. The only one which showed a marked change from the heterogeneous model was the slow timescale of the SSD of the HB species, $t_{2,HB}$, which tended to be faster by a factor of three. This is likely a

result of having less density from the exchange peaks at moderate times between 10 and 100 ps, so part of the SSD had to become faster to describe the observed decay.

The “jump” angle Θ did undergo a significant change, increasing from the $45^\circ \pm 5^\circ$ to about $60^\circ \pm 5^\circ$, although there was once again no significant temperature dependence. Per Eq. 4, this shifts the observed anisotropic decay from being slower than the exchange rate in the heterogeneous model to being faster than the exchange rate in the “wobbling” model. This change is likely in conjunction with complementary changes in the “wobbling” cone order parameter, S^2 , the direct analogue to the fraction f of the population undergoing slow exchange in the heterogeneous model. The predicted amplitude of the restricted angle wobbling motions were necessarily smaller than the corresponding fast population fraction, as they contribute less to the observed polarization dependence than the analogous large angle motion in the heterogeneous model. The smaller contribution from wobbling allows more contribution from the slow, large-angle exchange, which does produce the large polarization dependence in the CLS decays.

Table S1: Homogeneous “Wobbling” Kinetic Model Fit Parameters

τ_{ex} corresponds to $1/k_{NB-HB}$. S^2 , T^2 , and τ_{wob} correspond to what appears in Eq. S6.

T (K)	Θ (°)	$\log[\tau_{ex}/ps]^a$	S^2	$\log[\tau_{wob}/ps]$	T^2
355	47 ± 12	1.6 ± 0.1	0.35 ± 0.06	1.2 ± 0.07	0.82 ± 0.01
345	63 ± 7	1.8 ± 0.1	0.51 ± 0.06	1.0 ± 0.1	0.89 ± 0.02
335	65 ± 13	1.9 ± 0.1	0.54 ± 0.06	0.9 ± 0.1	0.94 ± 0.02
325	58 ± 7	1.9 ± 0.1	0.56 ± 0.04	0.8 ± 0.2	0.84 ± 0.02
315	60 ± 6	2.2 ± 0.1	0.63 ± 0.03	0.9 ± 0.1	0.91 ± 0.02
300	52 ± 3	2.5 ± 0.1	0.63 ± 0.02	1.3 ± 0.1	0.83 ± 0.01
290	53 ± 4	2.6 ± 0.1	0.76 ± 0.01	1.0 ± 0.3	0.89 ± 0.02
280	63 ± 13	3.2 ± 0.1	0.78 ± 0.02	1.4 ± 0.2	0.95 ± 0.01
270	58 ± 19	3.7 ± 0.4	0.77 ± 0.04	1.5 ± 0.4	0.92 ± 0.02

S8. Plots of Homogeneous and Heterogeneous Model Fits at All Temperatures

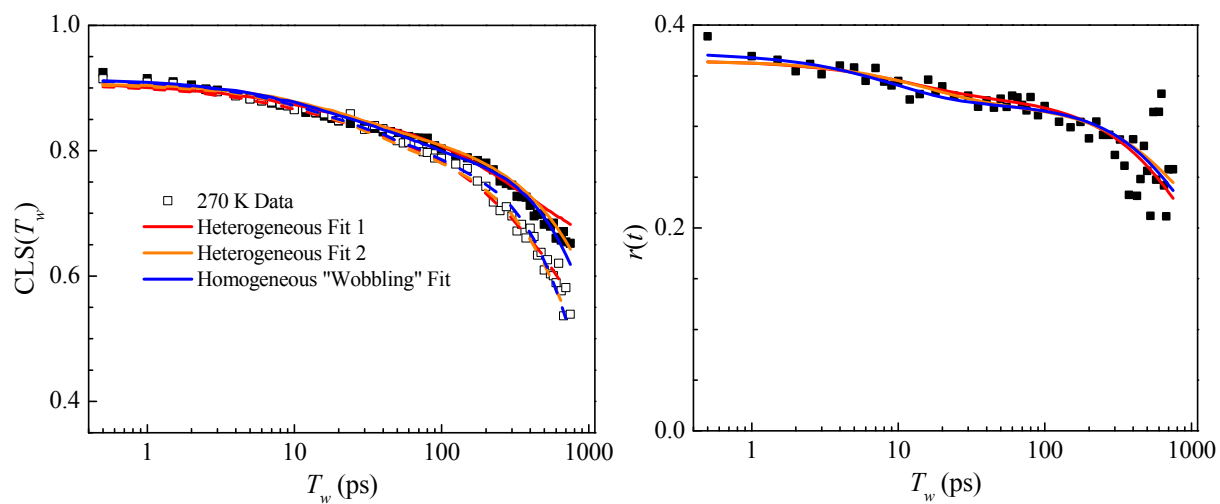


Fig. S2: 270 K

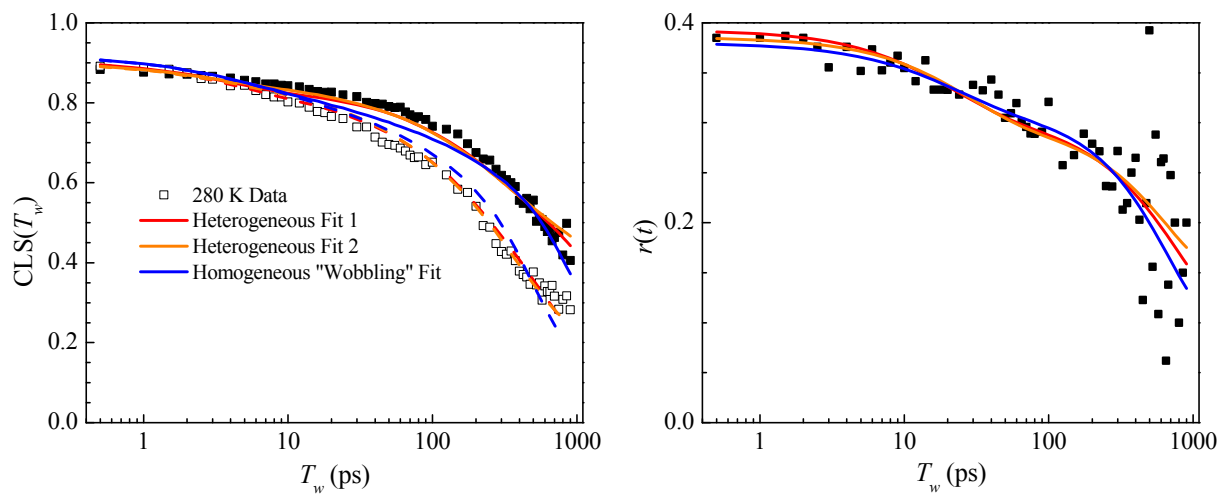


Fig S3: 280 K

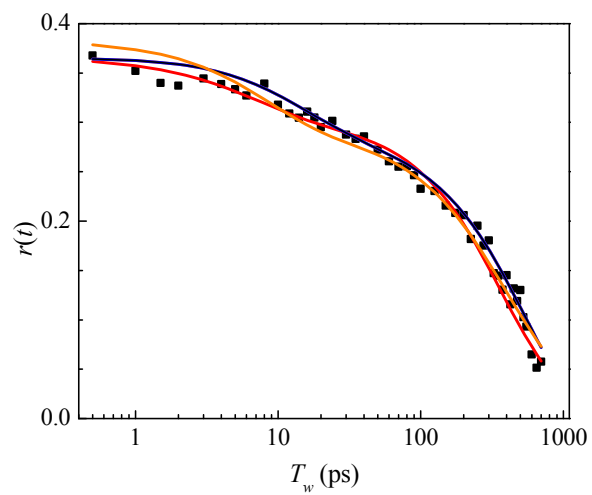
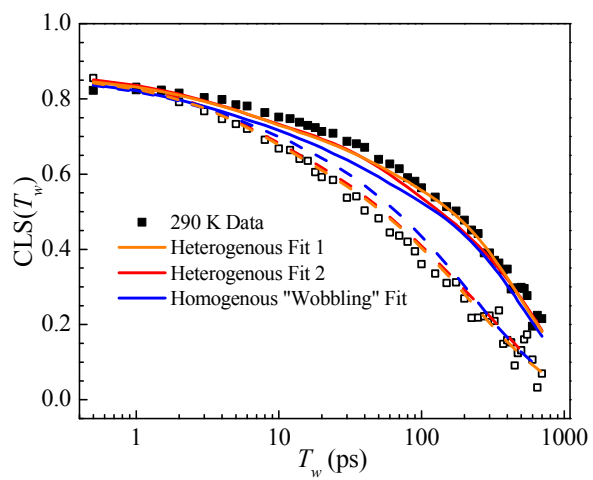


Fig. S4: 290 K

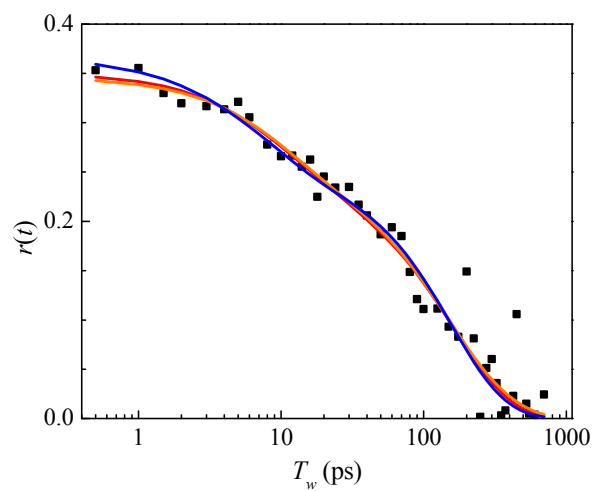
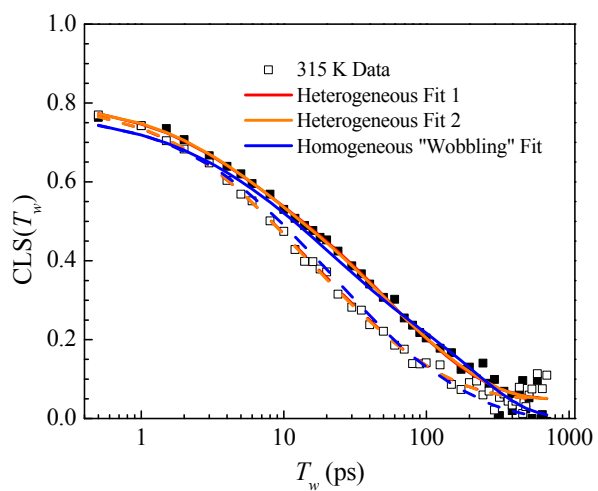


Fig. S5: 315 K

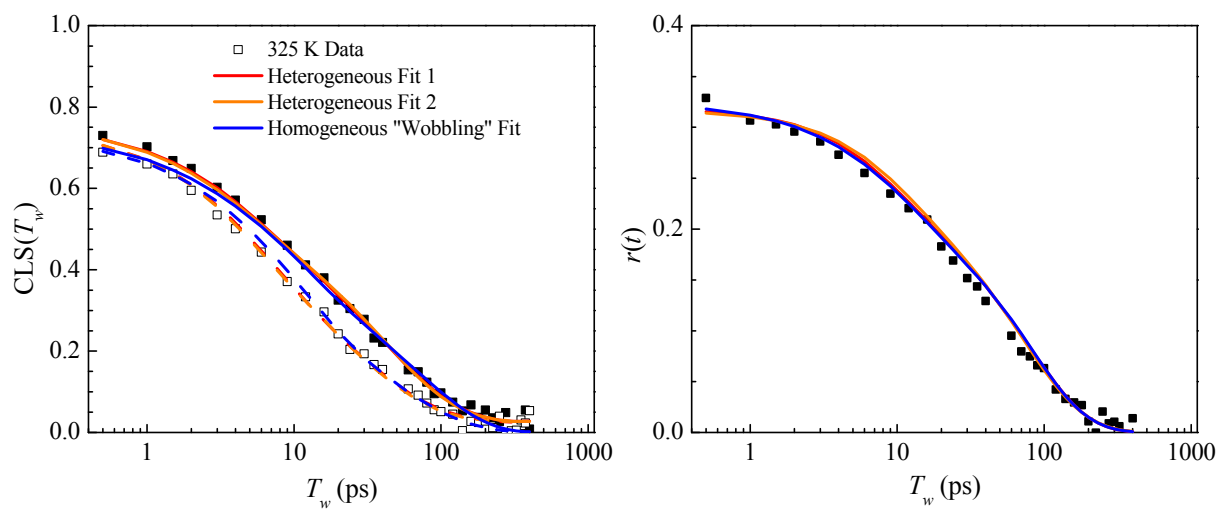


Fig. S6: 325 K

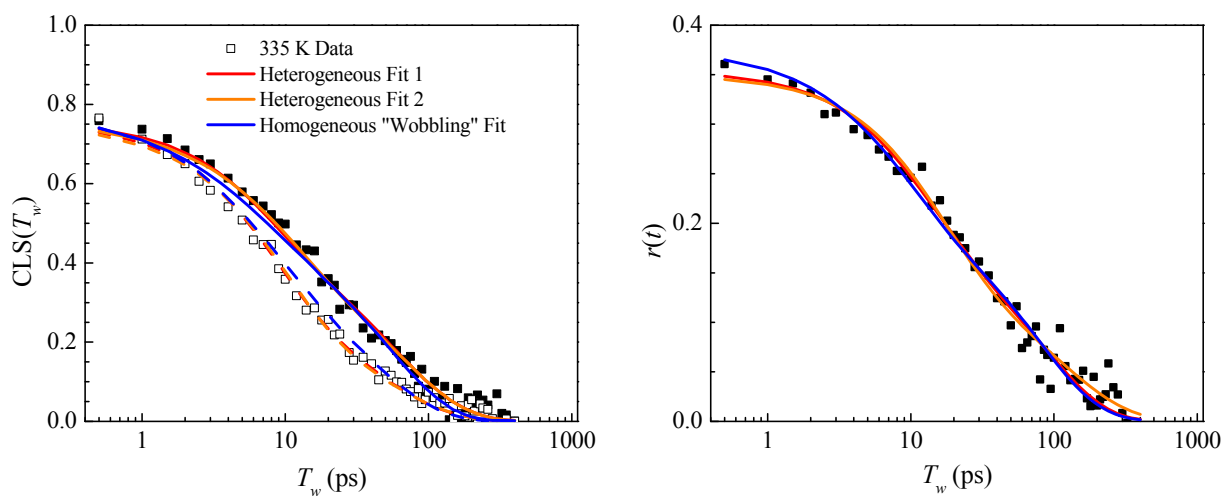


Fig S7: 335 K

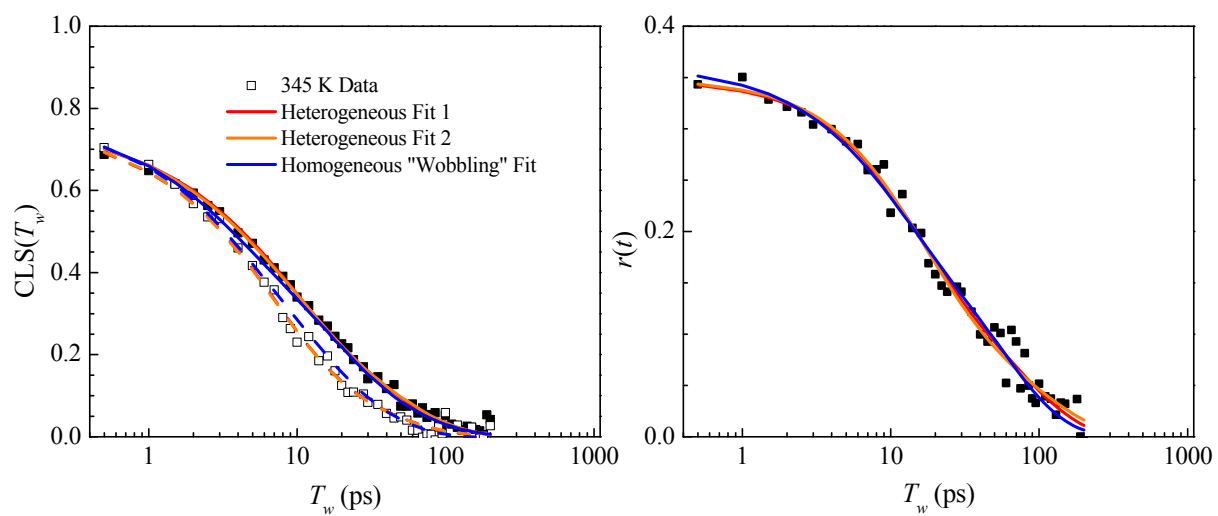


Fig. S8: 345 K

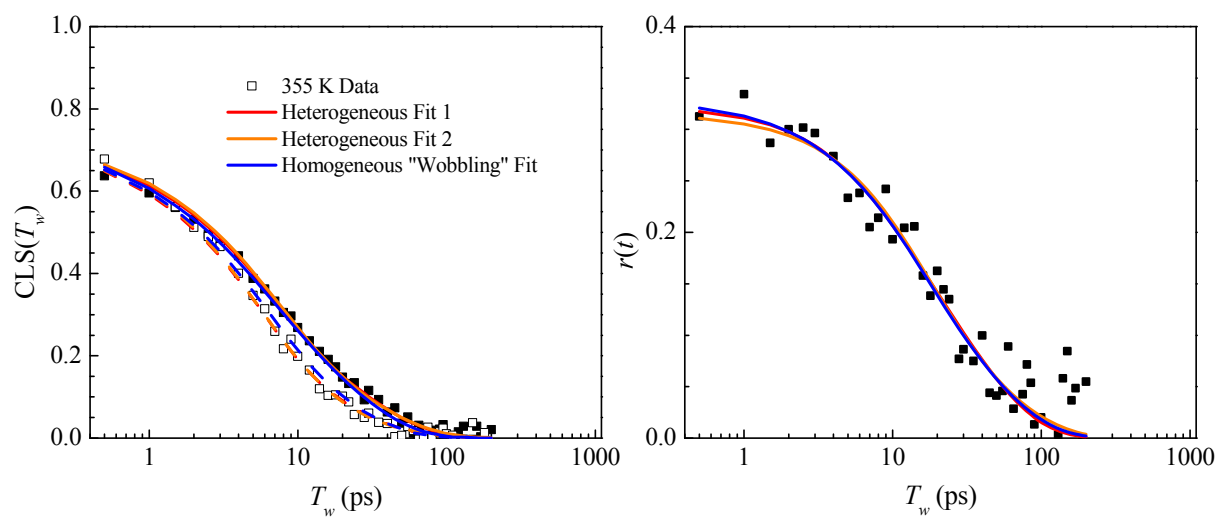


Fig S9: 355 K

References

1. M. Ji and K. J. Gaffney, *J. Chem. Phys.* **134**, 044516 (2011).
2. K. Kwak, J. Zheng, H. Cang and M. D. Fayer, *J. Phys. Chem. B* **110**, 19998-20013 (2006).
3. D. J. Hoffman and M. D. Fayer, *J. Phys. Chem. B* **121**, 10417-10428 (2017).
4. D. J. Hoffman, K. P. Sokolowsky and M. D. Fayer, *J. Chem. Phys.* **146** (12), 124505 (2017).
5. P. Hamm and M. Zanni, *Concepts and methods of 2D infrared spectroscopy*. (Cambridge University Press, 2011).
6. G. Lipari and A. Szabo, *Biophys. J.* **30**, 489-506 (1980).
7. G. Lipari and A. Szabo, *J. Am. Chem. Soc.* **104**, 4546-4559 (1982).
8. R. B. Williams, R. F. Loring and M. D. Fayer, *J. Phys. Chem. B* **105**, 4068-4071 (2001).
9. K. A. Merchant, W. G. Noid, R. Akiyama, I. Finkelstein, A. Goun, B. L. McClain, R. F. Loring and M. D. Fayer, *J. Am. Chem. Soc.* **125**, 13804-13818 (2003).
10. S. Bagchi, S. G. Boxer and M. D. Fayer, *J. Phys. Chem. B* **116**, 4034-4042 (2012).
11. K. D. Rector and M. D. Fayer, *J. Chem. Phys.* **108**, 1794-1803 (1998).
12. R. M. MacFarlane and R. M. Shelby, *J. Lumin.* **36**, 179-207 (1987).